



HAL
open science

High-resolution vacuum ultraviolet absorption spectra of 2,3- and 2,5-dihydrofuran

Anja Röder, Nelson de Oliveira, Floriane Grollau, Jean-Michel Mestdagh,
Guillaume Gallician, Marc-André Gaveau, Laurent Nahon, Marc Briant

► To cite this version:

Anja Röder, Nelson de Oliveira, Floriane Grollau, Jean-Michel Mestdagh, Guillaume Gallician, et al.. High-resolution vacuum ultraviolet absorption spectra of 2,3- and 2,5-dihydrofuran. The Journal of Chemical Physics, 2020, 153 (13), pp.134303. 10.1063/5.0015835 . cea-02962478

HAL Id: cea-02962478

<https://cea.hal.science/cea-02962478>






Submitted on 14 Feb 2024

HAL is a multi-disciplinary open access archive for the deposit and dissemination of scientific research documents, whether they are published or not. The documents may come from teaching and research institutions in France or abroad, or from public or private research centers.

L'archive ouverte pluridisciplinaire **HAL**, est destinée au dépôt et à la diffusion de documents scientifiques de niveau recherche, publiés ou non, émanant des établissements d'enseignement et de recherche français ou étrangers, des laboratoires publics ou privés.

RESEARCH ARTICLE | OCTOBER 01 2020

High-resolution vacuum ultraviolet absorption spectra of 2,3- and 2,5-dihydrofuran

Anja Röder ; Nelson de Oliveira; Floriane Grollau; Jean-Michel Mestdagh ; Guillaume Gallician ; Marc-André Gaveau; Laurent Nahon ; Marc Briant 



J. Chem. Phys. 153, 134303 (2020)

<https://doi.org/10.1063/5.0015835>



View
Online



Export
Citation

CrossMark



The Journal of Chemical Physics
2024 Emerging Investigators
Special Collection

Submit Today

High-resolution vacuum ultraviolet absorption spectra of 2,3- and 2,5-dihydrofuran

Cite as: J. Chem. Phys. 153, 134303 (2020); doi: 10.1063/5.0015835

Submitted: 30 May 2020 • Accepted: 16 September 2020 •

Published Online: 1 October 2020





View Online



Export Citation



CrossMark

Anja Röder,^{1,2,a)}  Nelson de Oliveira,³ Floriane Grollau,⁴ Jean-Michel Mestdagh,⁴ 
Guillaume Gallician,⁴  Marc-André Gaveau,⁴ Laurent Nahon,³  and Marc Briant⁴ 

AFFILIATIONS

¹Department of Chemistry, University of Ottawa, 10 Marie Curie, Ottawa, Ontario K1N 6N5, Canada

²Joint Centre for Extreme Photonics, National Research Council and University of Ottawa, Ottawa, Ontario K1A 0R6, Canada

³Synchrotron Soleil, Orme des Merisiers, St. Aubin BP48, 91192 Gif-sur-Yvette Cedex, France

⁴Université Paris-Saclay, CEA, CNRS, LIDYL, 91191 Gif-sur-Yvette, France

^{a)} Author to whom correspondence should be addressed: roeder.anja.sci@gmail.com

ABSTRACT

Using a synchrotron-based Fourier-transform spectrometer, the high-resolution absorption spectra of the C_{1v} -symmetric 2,3-dihydrofuran (23DHF) and C_{2v} -symmetric 2,5-dihydrofuran (25DHF) have been measured from 5.5 eV to 9.4 eV with an absolute absorption cross section scale. Oscillator strengths and vertical excitation energies of the lowest 18 states have been computed using the average of the second- and third-order algebraic diagrammatic construction polarization propagator method and the equation-of-motion coupled-cluster method at the level of singles and doubles model. These show that the bright valence transitions of $\pi\pi^*$ -character are embedded into Rydberg transitions, whose oscillator strengths are at least one order of magnitude lower. To account for intensity borrowing, the first broad valence transition between 5.5 eV and 6.8 eV was simulated using a nuclear ensemble, and the agreement between experiment and theory is excellent. Whereas 23DHF only exhibits one broad valence transition followed by d/f Rydberg series converging to the ionization energy, the absorption spectrum of 25DHF has four bands, attributed to a valence $n\pi\sigma \rightarrow \pi^*$ -transition, $n\pi\sigma \rightarrow 3p_{xz}/3d_{xz}$ transitions, a second valence $n\pi \rightarrow \pi^*$ -transition followed by d/f Rydberg series converging to the ionization energy, respectively. All Rydberg series converging to the ionization energy have been characterized in terms of their quantum defects.

Published under license by AIP Publishing. <https://doi.org/10.1063/5.0015835>

I. INTRODUCTION

2,3-Dihydrofuran (23DHF) and 2,5-dihydrofuran (25DHF) both possess the same chromophoric units: a C=C double bond and an oxygen atom. They differ only in the location of the double bond: in 23DHF, the double bond is a direct neighbor of the oxygen atom, whereas in 25DHF, CH₂ units separate the double bond from the oxygen atom (see Fig. 1 for the molecular structures). Their symmetries differ vastly: while 25DHF is C_{2v} -symmetric, in 23DHF, one CH₂-unit is distorted out of plane, resulting in C_{1v} -symmetry. From a symmetry point of view, 25DHF is more similar to furan,¹ albeit 23DHF is more similar to the completely saturated counterpart tetrahydrofuran (C_2 -symmetric).²

In both cases, their absorption spectra should be dominated by a bright valence $\pi \rightarrow \pi^*$ transition embedded in Rydberg manifolds. The difference in symmetry between 23DHF and 25DHF, however, should strongly impact the allowed transitions and coupling between excited-states. Previously, only the relative absorbance between 5.1 eV and 6.5 eV of 23DHF and 25DHF has been measured in a study focusing on the ring-opening dynamics,³ attributing the observed broad band in this region to $\pi\pi^*$ and $\pi 3s$ -Rydberg transitions. Excitation into this broad band leads to an ultrafast deactivation to the ground state via a conical intersection and ring-opening.³ Indeed, the linewidth of an electronic transition is an indicator of the underlying excited-state dynamics, as ultrafast dynamics in the temporal domain translates to broad bands in the

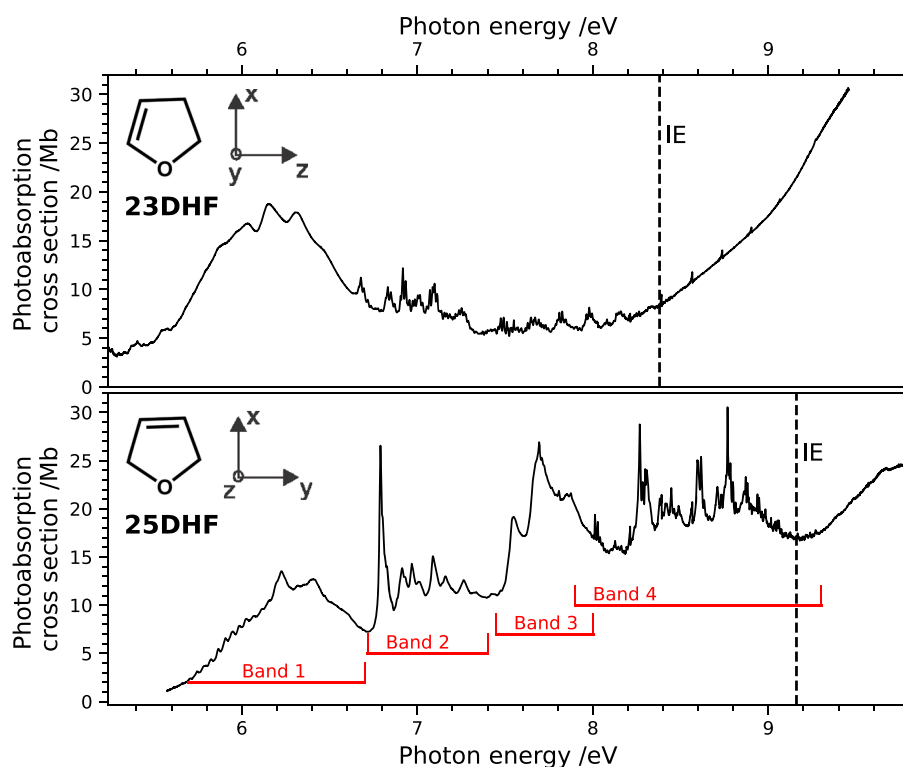


FIG. 1. VUV absorption spectra of 23DHF (top) and 25DHF (bottom). The vertical dashed lines correspond to the vertical ionization energies (IE) of 23DHF and 25DHF.³²

frequency domain, assuming that the molecules are not vibrationally or Doppler-broadened.

In the following, we present the absorption spectra all the way past the ionization energy (IE) including their absolute absorption cross sections and attribute the observed bands using high-level *ab initio* quantum calculations.

II. EXPERIMENT

The photoabsorption spectra of 23DHF and 25DHF were measured using the Fourier Transform Spectrometer (FTS),⁴ one of the permanent endstations of the VUV beamline DESIRS⁵ at the SOLEIL synchrotron radiation source. Detailed descriptions of the beamline and experimental setup have been given elsewhere.^{6,7}

In brief, highly coherent radiation spanning the whole VUV range, and for this study the ≈ 5.5 eV–10 eV range, is provided by a 14-period undulator, whose 7% bandwidth spectrum can be easily tuned. The beam is subsequently reflected by the beamline's mirrors toward the sample chamber of the FT spectroscopy experimental branch, before feeding the FTS. Two different absorption cell setups were used: (a) a windowless cell employing long entrance and exit capillaries, allowing for a renewed column of gas that is avoiding accumulation of photodissociation products. The whole relative absorption spectra of both substances were measured and assembled from the individual, overlapping spectral windows (undulator settings) using this cell. (b) A MgF₂-windowed cell of known

column density to determine the absolute photoabsorption cross section over several limited energy ranges, serving as a calibration for the absorption spectrum obtained from the windowless cell. Both cells were filled with either 23DHF or 25DHF vapor obtained from a liquid, room-temperature sample situated outside the vacuum chamber. 23DHF and 25DHF were purchased from Sigma-Aldrich. Before use, the liquid sample was subjected to several freeze–pump–thaw cycles. The absorption spectra were linearized following the Beer–Lambert law, using empty cell spectra as backgrounds. The absolute cross section scale was set using the spectral windows recorded with the windowed cell setup. We estimate an experimental uncertainty of the absolute absorption cross sections of $\pm 10\%$.⁶ The FTS spectral resolution was set to 8.6 cm^{-1} , very far from its ultimate bandwidth of $\leq 0.1\text{ cm}^{-1}$, since there was no need for a better spectral resolution as the narrowest structures observed in the spectra were already several times larger than the instrumental linewidth.

A molecular beam setup is also available on the FTS sample environment chamber^{6,7} at the same location as the cells mentioned above. Unfortunately, the sample density was too low in the beam for any absorbance to be observed.

III. COMPUTATIONAL DETAILS

All calculations employed the Qchem 4.4 package.⁸ Ground state structures were optimized using Density Functional Theory (DFT)⁹ with the cam-b3lyp functional¹⁰ employing an aug-cc-pVTZ

basis set (see Tables 1–5 of the [supplementary material](#)). Vibrational frequencies of the optimized ground state structures were calculated using cam-b3lyp/aug-cc-pVTZ.

Quantitative calculations of the vertical excitation energies of excited-states with Rydberg character would require a basis set with diffuse functions, and of course, the number of added functions should be larger for $n > 3$ than for $n = 3$ Rydberg states. The present aim is to quantitatively reproduce s-, p-, and d-Rydberg states with $n = 3$, for which an aug-cc-pVDZ basis set proved sufficient. Negligible changes in vertical excitation energies (see Tables 8 and 9 of the [supplementary material](#)) are observed when adding Rydberg functions to the basis set. The latter were placed on the molecular center of gravity according to Kaufman *et al.*¹¹ Increasing the basis set from aug-cc-pVDZ to aug-cc-pVTZ increased the vertical excitation energies of Rydberg and valence states by ~ 0.2 eV and 0.06 eV, respectively, but also considerably increased the calculation time especially for higher-lying states. As the order of excited states remained the same, the aug-cc-pVDZ basis set was deemed sufficient to allow assignment of the VUV absorption spectrum. The error associated with the excitation energies of 3f-Rydberg states is higher than those of 3s-, 3p-, and 3f-Rydberg states, as no f-type orbitals are included in the aug-cc-pVDZ basis set. The same basis was used to describe Rydberg states with $n > 3$. The purpose here is not to be quantitative but to serve as a guideline to explore which Rydberg series are symmetry-forbidden or allowed. The corresponding vertical excitation energies should be considered as qualitative (i.e., larger errors in excitation energies as compared to 3s-, 3p-, and 3d-Rydberg states).

Based on these optimized electronic ground state structures, the vertical excitation energies and oscillator strengths were calculated using Time-Dependent Density Functional Theory (TDDFT)¹² with the b3lyp,¹⁰ cam-b3lyp,¹³ pbe,¹⁴ and pbe0¹⁵ functionals, using the Algebraic Diagrammatic Construction polarization propagator through second order [ADC(2)], Algebraic Diagrammatic Construction polarization propagator through third order [ADC(3)],^{16–21} and Equation-Of-Motion Coupled-Cluster method at the levels of Singles and Doubles model (EOM-CCSD)²² with an aug-cc-pVDZ²³ basis set. The mean errors associated with ADC(2) (0.64 eV) and ADC(3) (0.2 eV), based on vertical excitation energies of H₂O, Ne, HF, and N₂,²⁰ have recently been revised to 0.16 eV and 0.21 eV, respectively, based on several hundred vertical excitation energies of small- and medium-sized molecules.²⁴ Reference 24 also suggested that the mean error of Rydberg and valence states could be reduced to 0.08 eV by taking the mean of the ADC(2) and ADC(3) values for states of the same excited-state character, called ADC(2.5). Following the latter suggestion, ADC(2.5) values are given below [ADC(2) and ADC(3) results can be found in Tables 10–12 of the [supplementary material](#)]. Even though the benchmark study using ADC(2.5) demonstrated that this approach significantly reduces the mean error,²⁴ its application is not yet widely spread. We therefore compare the ADC(2.5) results to vertical excitation energies calculated at the EOM-CCSD level, whose mean errors of the vertical excitation energies calculated at the EOM-CCSD level are usually conservatively estimated at 0.3 eV.⁸ The nature of the vertical excitation transitions was characterized in terms of Natural Transition Orbitals (NTOs).²⁵

Although vertical excitation energies and oscillator strength help greatly in assigning the measured bands, it ignores coupling

between excited states and the geometry distribution of the room-temperature vapor sample. To get such information qualitatively, we followed a recently used strategy where the first absorption band was simulated by considering an ensemble of nuclear geometries, assuming that the spectral band shape is determined by the ground-state nuclear geometry distribution (e.g., Refs. 26–29). This was achieved for the two molecules. 500 initial conditions were generated from a harmonic oscillator Wigner distribution at 293 K with Newton-X^{30,31} and the vertical excitation energies at each geometry calculated with cam-b3lyp using Qchem 4.4.⁸ The cam-b3lyp functional best represents the ordering and energy difference in comparison with ADC(2.5) and EOM-CCSD calculations. The resulting vertical excitation energies were convoluted with a Gaussian with a full-width at half-maximum of 0.04 eV in order to obtain a smooth curve.

IV. RESULTS

A. Experiment

The vacuum ultraviolet absorption spectra of 23DHF and 25DHF (top and bottom of Fig. 1, respectively) are quite different. Whereas 23DHF exhibits one broad band centered around 6 eV followed by less intense features, 25DHF shows four main and quite structured bands centered at 6.2 eV, 7.0 eV, 7.7 eV, and 8.5 eV, respectively. These features will be discussed separately. Assignments and positions of individual peaks can be found in the [supplementary material](#).

B. Calculations

1. Ground state structures

Two structures have been proposed for the ground state of 23DHF: a C_S structure and a puckered C₁-structure, where one CH₂-group is distorted out of the plane of the ring. IR spectra^{33–35} and microwave spectra³⁶ have shown that two C₁-symmetric minima are separated by a barrier of 93.4 cm⁻¹, which corresponds to a C_S-structure³⁴ (see Fig. 2 for a schematic representation). This barrier is only slightly larger than the zero-point vibrational energy of the ring

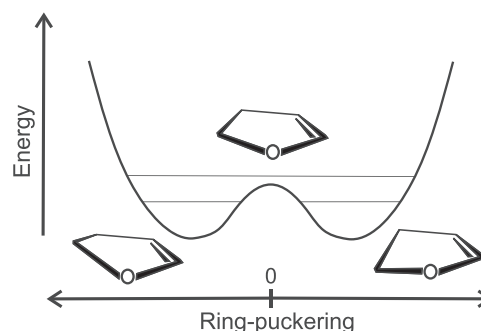


FIG. 2. Schematic representation of the double-well ground state along the ring-puckering coordinate of 23DHF. The C₁- and C_S-symmetric structures of 23DHF are represented schematically, with the out-of-plane deformation exaggerated for a better representation.

puckering motion ν_{27} of 75 cm^{-1} , showing that the ground vibrational level is very close to this barrier. A floppy structure is therefore expected. The corresponding vibrational wave function is likely complex. It necessarily involves out of plane deformations. Hence, to mimic the absorption spectrum quantitatively, vertical excitation energies must be evaluated for the stationary points of C_1 and C_s symmetry along the corresponding deformation coordinate. Their weight, based on the barrier height, is provided by the Boltzmann population of the C_1 and C_s species at 293 K (61.3% and 38.7%, respectively).

Our calculated ground state structures agree with the prevailing assessments in the literature: both cam-b3lyp/aug-cc-pVDZ and MP2/aug-cc-pVDZ ground state geometry optimizations show that C_1 -symmetric 23DHF is energetically lower than C_s -symmetric 23DHF. Moreover, C_s -symmetric 23DHF has one imaginary ring-puckering frequency, identifying it as a transition state.

25DHF, on the other hand, is C_{2v} -symmetric, in agreement with IR spectra measurements.^{35,37,38} Our calculated ground state structures optimized at the cam-b3lyp/aug-cc-pVDZ and MP2/aug-cc-pVDZ level of theory are C_{2v} -symmetric with no imaginary frequencies.

2. Excited states of 23DHF

In the following, we will start with discussing first the vertical excitations of C_1 -symmetric 23DHF calculated at the ADC(2.5)/aug-cc-pVDZ and EOM-CCSD/aug-cc-pVDZ level of theory (see Table I, left and center).

The Highest Occupied Molecular Orbitals (HOMOs) and Lowest Unoccupied Molecular Orbitals (LUMOs) of the ground state Hartree-Fock electronic configuration of 23DHF (C_1) can be characterized as follows:

$$\begin{aligned} \text{HOMO: } & (18a(\sigma))^2(19a(\pi))^2 \text{ and} \\ \text{LUMOs: } & (20a(3s))^0(21a(3p_z))^0(22a(3p_x))^0(23a(3p_y))^0 \\ & (24a(3d_{xz}))^0(25a(3d_z))^0(26a(\pi^*))^0(27a(3d_{x^2-y^2}))^0. \end{aligned}$$

In agreement with this electronic configuration, the first four vertical excitations correspond to electronic transitions from a π -orbital electron toward the 3s and 3p Rydberg orbitals, with the transition into the $3p_y$ having the most oscillator strength. The next transition has $\pi \rightarrow \pi^*$ character, and its oscillator strength is at least a factor of 2 higher than all other vertical excitations. Following the $\pi \rightarrow \pi^*$ transition, there are excitations of a π -electron to the 3d, 4f, and even 5g Rydberg orbitals, as well as some transitions starting from the HOMO-1 σ -orbital into the 3s Rydberg orbital. Until state 13A, ADC(2.5) and EOM-CCSD calculations are in excellent agreement, predicting the same ordering of excited states. The energies calculated at the EOM-CCSD level lie, in general, about 0.15 eV higher. After state 14A, the order of the states differs between the ADC(2.5) and EOM-CCSD calculations, but the manifold of states is now very dense and the relative energy difference between states of the same character remains within 0.2 eV. The order and character of the excited states remain unchanged when comparing C_1 - to C_s -symmetric 23DHF, and the vertical excitation energies change only around 0.05 eV, which is negligible. This shows that the C_1 -structure

TABLE I. Symmetries, vertical excitation energies E , oscillator strengths f , and character assignments of the first 18 excited states of 23DHF at C_1 (C_s) calculated at the ADC(2.5)/aug-cc-pVDZ, EOM-CCSD/aug-cc-pVDZ, and cam-b3lyp/aug-cc-pVDZ level of theory. The oscillator strengths of ADC(2.5) correspond to the oscillator strengths calculated at the ADC(3)/aug-cc-pVDZ level of theory. ADC(2.5) vertical excited states correspond to the mean of ADC(2) and ADC(3) vertical excited states of the same transition character, calculated with the aug-cc-pVDZ basis set. See the [supplementary material](#) for the numerical values of the ADC(2) and ADC(3) calculations.

Sym.	ADC(2.5)/aug-cc-pVDZ			EOM-CCSD/aug-cc-pVDZ			cam-b3lyp/aug-cc-pVDZ		
	E (eV)	$f(10^{-3})$	Assignment	E (eV)	$f(10^{-3})$	Assignment	E (eV)	$f(10^{-3})$	Assignment
2A (1A'')	5.31 (5.25)	17 (17)	$\pi \rightarrow 3s$	5.45 (5.40)	14 (13)	$\pi \rightarrow 3s$	5.31 (5.25)	14 (14)	$\pi \rightarrow 3s$
3A (2A'')	5.97 (5.94)	9 (7)	$\pi \rightarrow 3p_z$	6.13 (6.10)	6 (5)	$\pi \rightarrow 3p_z$	5.95 (5.92)	6 (5)	$\pi \rightarrow 3p_z$
4A (2A')	6.03 (6.01)	51 (44)	$\pi \rightarrow 3p_y$	6.19 (6.17)	28 (21)	$\pi \rightarrow 3p_y$	6.03 (6.00)	35 (28)	$\pi \rightarrow 3p_y$
5A (3A'')	6.10 (6.07)	3 (1)	$\pi \rightarrow 3p_x$	6.26 (6.22)	1 (1)	$\pi \rightarrow 3p_x$	6.10 (6.07)	2 (1)	$\pi \rightarrow 3p_x$
6A (3A')	6.39 (6.41)	123 (141)	$\pi \rightarrow \pi^*$	6.59 (6.61)	118 (141)	$\pi \rightarrow \pi^*$	6.53 (6.58)	89 (166)	$\pi \rightarrow \pi^*$
7A (4A'')	6.57 (6.51)	10 (0)	$\pi \rightarrow 3d_z^2$	6.71 (6.64)	18 (0)	$\pi \rightarrow 3d_z^2$	6.61 (7.18)	70 (58)	$\pi \rightarrow 3d_{x^2-y^2}$ $\pi \rightarrow \pi^*$
8A (5A'')	6.75 (7.08)	5 (26)	$\pi \rightarrow 3d_{zx}$	6.91 (6.87)	5 (4)	$\pi \rightarrow 3d_{zx}$	6.72 (6.68)	9 (4)	$\pi \rightarrow 3d_{zx}$
9A (6A'')	7.28 (7.29)	30 (26)	$\pi \rightarrow 3d_{zy}$	7.22 (7.21)	29 (24)	$\pi \rightarrow 3d_{xy}$	7.07 (6.52)	35 (1)	$\pi \rightarrow 3d_z^2$
10A (4A')	7.16 (7.36)	33 (41)	$\pi \rightarrow 3d_{xy}$	7.44 (7.21)	33 (42)	$\pi \rightarrow 3d_{x^2-y^2}$	7.28 (7.47)	41 (28)	$\pi \rightarrow 3d_{zy}$
11A (5A')	7.41 (6.71)	26 (5)	$\pi \rightarrow 3d_{x^2-y^2}$	7.63 (7.59)	26 (26)	$\pi \rightarrow 3d_{zy}$	7.51 (7.07)	27 (25)	$\pi \rightarrow 3d_{xy}$
12A (7A'')	8.05 (8.01)	4 (5)	$\pi \rightarrow 4f_{y(3x^2-y^2)}$	8.20 (8.16)	2 (3)	$\pi \rightarrow 4f_{y(3x^2-y^2)}$	8.02 (7.98)	3 (4)	$\pi \rightarrow 4f_{y(3x^2-y^2)}$
13A (8A'')	8.20 (8.4)	3 (2)	$\pi \rightarrow 4f_{x(z^2-3y^2)}$	8.35 (8.32)	3 (2)	$\pi \rightarrow 4f_{x(z^2-3y^2)}$	8.17 (8.14)	3 (2)	$\pi \rightarrow 4f_{x(z^2-3y^2)}$
14A (9A'')	8.44 (8.40)	1 (0)	$\pi \rightarrow 4s$	8.60 (8.56)	1 (0)	$\pi \rightarrow 4s$	8.36 (8.32)	1 (0)	$\pi \rightarrow 4s$
15A (10A'')	8.68 (9.06)	1 (4)	$\pi \rightarrow 4f_z^3$	8.84 (9.03)	0 (6)	$\pi \rightarrow 4p_z$	8.63 (8.61)	1 (0)	$\pi \rightarrow 4f_z^3$
16A (6A')	8.72 (8.91)	7 (9)	$\sigma \rightarrow 3s$	8.87 (9.17)	7 (1)	$\pi \rightarrow 4f_{xz}^2$	8.67 (8.67)	6 (6)	$\pi \rightarrow 4f_{xz}^2$
17A (7A')	8.77 (...)	1 (...)	$\pi \rightarrow 4f_{xz}^2$	9.01 (...)	3 (...)	$\pi \rightarrow 5g_{x^4+y^4}$	8.78 (8.75)	0 (0)	$\pi \rightarrow 4f_{yz}^2$
18A (8A')	8.90 (...)	4 (...)	$\pi \rightarrow 5g_{x^4+y^4}$	9.05 (9.07)	11 (15)	$\sigma \rightarrow 3s$	8.81 (8.78)	3 (1)	$\pi \rightarrow 4p_z$
19A (9A')	8.93 (...)	30 (...)	$\pi \rightarrow 5g_{xy(x^2-y^2)}$	9.07 (9.03)	7 (6)	$\pi \rightarrow 4p_z$	8.89 (8.92)	6 (14)	$\sigma \rightarrow 3s$

is close to the C_s -structure, as the dihedral $CH-O-CH_2-CH_2$ angle is only 21° .

In order to simulate the first absorption band using an ensemble of nuclear geometries, we need a computationally cheap method that still properly represents the order and relative energy gaps between the first five excited states. In Table 13 of the [supplementary material](#), the vertical excitation energies and characters of different TDDFT functionals are compared to the ADC(2.5)-results for 23DHF. Besides cam-b3lyp, all other tested functionals predict the $\pi \rightarrow \pi^*$ -transition to lie above several 3d-Rydberg states, and the relative energy gap of the $\pi \rightarrow 3s$ and $\pi \rightarrow \pi^*$ is with 1.37 eV–2.44 eV higher than for ADC(2.5) (1.08 eV). Cam-b3lyp predicts an energy of 1.22 eV, which is much closer to the one predicted by ADC(2.5), and the $\pi \rightarrow \pi^*$ -transition follows directly after transitions into the 3p Rydberg manifold. It should be noted that the 7A transition also has $\pi \rightarrow \pi^*$ character besides $\pi \rightarrow 3d_{x^2-y^2}$ -character, indicating that those two states might be strongly coupled. The $\pi \rightarrow \pi^*$ transition is then followed by transitions into the d-Rydberg manifold. Even though this is different from the ADC(2.5) calculations, the cam-b3lyp functional still represents best the order

and energy gap for 23DHF and was therefore chosen to simulate the first absorption band of 23DHF, incorporating the first six states.

It should be noted that calculations are in agreement with the previous δ -CR-EOMCCSD(T)/aug-cc-pVDZ calculations by Schalk *et al.*,³ which predict the 3s and 3p_{x,y} transitions to be lower in energy than the $\pi \rightarrow \pi^*$ -character transitions. They predict two transitions with $\pi\pi^*$ -character, with one having negligible oscillator strength, similar to our cam-b3lyp/aug-cc-pVDZ calculations. They, however, assume a C_s geometry for the 23DHF ground state, which can influence the mixing between different states and their relative oscillator strengths—as seen in our cam-b3lyp/aug-cc-pVTZ calculations for states 6A and 7A when changing the geometry from C_1 to C_s .

3. Excited states of 25DHF

The HOMOs and LUMOs of 25DHF can be characterized as follows:

TABLE II. Symmetries, vertical excitation energies E , oscillator strengths f , and character assignments of the first 18 excited states of 25DHF calculated at the ADC(2.5)/aug-cc-pVDZ, EOM-CCSD/aug-cc-pVDZ, and cam-b3lyp/aug-cc-pVDZ level of theory. The oscillator strengths of ADC(2.5) correspond to the oscillator strengths calculated at the ADC(3)/aug-cc-pVDZ level of theory. ADC(2.5) vertical excited states correspond to the mean of ADC(2) and ADC(3) vertical excited states of same transition character, calculated with the aug-cc-pVDZ basis set. See the [supplementary material](#) for the numerical values of the ADC(2) and ADC(3) calculations.

N state	ADC(2.5)/aug-cc-pVDZ				EOM-CCSD/aug-cc-pVDZ				cam-b3lyp/aug-cc-pVDZ			
	Sym.	E (eV)	f (10^{-3})	Assignment	Sym.	E (eV)	f (10^{-3})	Assignment	Sym.	E (eV)	f (10^{-3})	Assignment
1	1B ₂	5.97	0.6	$n\pi\sigma \rightarrow 3s$	1B ₂	6.16	0.6	$n\pi\sigma \rightarrow 3s$	1B ₂	5.94	0.4	$n\pi\sigma \rightarrow 3s$
2	1B ₁	6.55	184	$n\pi\sigma \rightarrow \pi^*$	1B ₁	6.82	100	$n\pi\sigma \rightarrow \pi^*$	1B ₁	6.36	114	$n\pi\sigma \rightarrow \pi^*$
3	1A ₂	6.64	0	$n\pi\sigma \rightarrow 3p_y$	1A ₂	6.85	0	$n\pi\sigma \rightarrow 3p_y$	1A ₂	6.60	0	$n\pi\sigma \rightarrow 3p_y$
4	2B ₂	6.73	26	$n\pi\sigma \rightarrow 3p_x$	2B ₂	6.88	16	70% $n\pi\sigma \rightarrow 3p_x$ 20% $n\pi \rightarrow 3s$	2B ₂	6.63	23	$n\pi\sigma \rightarrow 3p_x$
5	2A ₁	6.78	16	$n\pi\sigma \rightarrow 3p_z$	2A ₁	6.98	6	$n\pi\sigma \rightarrow 3p_z$	2A ₁	6.76	10	$n\pi\sigma \rightarrow 3p_z$
6	3B ₂	7.18	18	$n\pi\sigma \rightarrow 3d_{xz}$	3B ₂	7.34	32	$n\pi\sigma \rightarrow 3d_{xy}$	3B ₂	7.13	19	$n\pi\sigma \rightarrow 3d_{xy}$
7	2A ₂	7.40	0	$n\pi\sigma \rightarrow 3d_{x^2-y^2}$	2A ₂	7.59	0	$n\pi\sigma \rightarrow 3d_{x^2-y^2}$	2A ₂	7.31	0	$n\pi\sigma \rightarrow 3d_{x^2-y^2}$
8	4B ₂	7.54	0	$n\pi \rightarrow 3s$	4B ₂	7.60	11	70% $n3s$ 15% $n\pi\sigma \rightarrow 3p_x$	4B ₂	7.43	17	$n\pi \rightarrow 3s$
9	2B ₁	7.54	46	$n\pi\sigma \rightarrow 3d_{yz}$	2B ₁	7.75	37	$n\pi\sigma \rightarrow 3d_{xz}$	2B ₁	7.45	26	$n\pi\sigma \rightarrow 3d_{yz}$
10	5B ₂	7.64	29	$n\pi\sigma \rightarrow 3d_z^2$	5B ₂	7.82	0.9	$n\pi\sigma \rightarrow 3d_z^2$	5B ₂	7.62	1	$n\pi\sigma \rightarrow 3d_z^2$
11	3A ₁	8.15	27	$n\pi \rightarrow 3p_z$	3A ₁	8.20	36	70% $n\pi 3d_{xz}$ 15% $n\pi\sigma \rightarrow 3p_z$	3A ₁	8.04	32	$n\pi \rightarrow 3p_z$
12	3A ₂	8.17	0	$n\pi \rightarrow 3p_y$	3A ₂	8.25	0	$n\pi \rightarrow 3p_y$	3A ₂	8.08	0	$n\pi \rightarrow 3p_y$
13	3B ₁	8.19	137	$n\pi \rightarrow \pi^*$	3B ₁	8.29	227	$n\pi \rightarrow \pi^*$	3B ₁	8.08	320	$n\pi \rightarrow \pi^*$
14	4A ₂	8.55	0	$\sigma \rightarrow \pi^*$	4A ₁	8.75	13	$\sigma \rightarrow 3s$	4A ₁	8.18	4	$n\pi \rightarrow 3p_x$
15	5A ₂	8.64	0	$n\pi\sigma \rightarrow 3d_{xy}$	4A ₂	8.75	0	53% $n\pi\sigma \rightarrow 4f_{x(x^2-3y^2)}$ 32% $n\pi \rightarrow 3d_{xy}$	4A ₂	8.30	0	$\sigma \rightarrow \pi^*$
16	4A ₁	8.65	11	$\sigma \rightarrow 3s$	5A ₁	8.85	0.2	71% $n\pi\sigma \rightarrow 3d_{xz}$ 15% $n\pi \rightarrow 3p_z$	5A ₁	8.47	3	80% $n\pi \rightarrow 3d_{xy}$ 20% $n\pi\sigma \rightarrow 4f_{x(x^2-3y^2)}$
17	5A ₁	8.65	0.1	$n\pi\sigma \rightarrow 3d_{xz}$	5A ₂	9.05	0	47% $n\pi\sigma \rightarrow 3d_{xy}$ 39% $n\pi \rightarrow 4f_{x(x^2-3y^2)}$	5A ₂	8.52	0	30% $n\pi \rightarrow 3d_{xy}$ 60% $n\pi\sigma \rightarrow 4f_{x(x^2-3y^2)}$
18	4B ₁	9.05	15	$n\pi \rightarrow 3d_{yz}$	4B ₁	9.11	0	$n\pi \rightarrow 3d_{yz}$	6A ₂	8.60	0	80% $n\pi\sigma \rightarrow 3d_{yz}$ 20% $n\pi \rightarrow 3p_z$

$$\begin{aligned} \text{HOMOs: } & (9a_1(\sigma))^2 (2b_2(n\pi))^2 (3b_2(n\pi\sigma))^2 \text{ and} \\ \text{LUMOs: } & (10a_1(3s))^0 (7b_1(3p_y))^0 (11a_1(3p_x))^0 (4b_2(3p_z))^0 \\ & (8b_1(3d_{x^2-y^2}))^0 (12a_1(\pi^*))^0 (13a_1(3d_{xz}))^0 (5b_2(3d_z^2))^0. \end{aligned}$$

In contrast to 23DHF, both HOMO and HOMO-1 of 25DHF possess mixed n and π -character (see Fig. 4 of the [supplementary material](#)), though the HOMO has significant contribution from σ molecular orbitals on the CH_2 -groups. Therefore, the HOMO is further referred to as $n\pi\sigma$ and the HOMO-1 as $n\pi$. The LUMOs, on the other hand, consist of a π^* embedded in a Rydberg manifold.

From a symmetry point of view, electronic transitions for the C_{2v} -symmetric 25DHF are classified into four irreducible representations: A_1 , A_2 , B_1 , and B_2 . A_2 is symmetry-forbidden, corresponding to $b_2 \rightarrow b_1$ transition from the HOMO/HOMO-1 to the LUMOs: transitions into $3p_y$ and $3d_{(x^2-y^2)}$ are therefore dark.

A list of the first 18 vertical excitation energies, oscillator strengths, and their assignments calculated at the ADC(2.5), EOM-CCSD, and cam-b3lyp level of theory with an aug-cc-pVDZ basis set is given in [Table II](#). Again, we will start the discussion considering only ADC(2.5) and EOM-CCSD results. Contrary to 23DHF, only the $n\pi\sigma \rightarrow 3s$ transition lies below the $n\pi\sigma \rightarrow \pi^*$ -transition, with a gap of about 0.58 eV and 0.66 eV for ADC(2.5) and EOM-CCSD, respectively. The oscillator strength of the $n\pi\sigma \rightarrow \pi^*$ -transition is nearly one order of magnitude larger than the surrounding transitions into the Rydberg manifold: we therefore expect this transition to dominate the first absorption band. This bright transition is followed by transitions from $n\pi\sigma$ into the $3p$ and $3d$ Rydberg manifold, before electron promotion from the lower-lying $n\pi$ molecular orbital starts to occur. After $n\pi \rightarrow 3s$ and $n\pi \rightarrow 3p_{z,y}$, follows the bright $n\pi \rightarrow \pi^*$ -transition, whose oscillator strength is on the same order of magnitude as the first $n\pi\sigma \rightarrow \pi^*$ -transition, albeit roughly 1.5 eV higher in energy. We therefore expect 25DHF to show two valence transitions into π^* -orbital, contrary to 23DHF. After this second valence transition, the manifold becomes dense, and the character assignments for EOM-CCSD and ADC(2.5) diverge. It is likely that this manifold of states is even denser, but only the first five excited states for each irreducible symmetry representation could be calculated as higher excited states failed to converge.

Just as observed in the excited-state calculations of 23DHF, EOM-CCSD energies are about 0.2 eV higher than those predicted by ADC(2.5), and states possess mixed character more often for EOM-CCSD. Overall, the agreement between both methods, especially up to state 14, is excellent. However, just as for 23DHF, in order to simulate the absorption spectrum of the first absorption band using a nuclear ensemble, we need a method which is computationally cheap yet describes the same order and energy gaps as the higher-level ADC(2.5) and EOM-CCSD methods. Comparing the vertical excitation energies and characters for different TDDFT functionals with ADC(2.5)-results (see [Table 14](#) of the [supplementary material](#)), the cam-b3lyp emerges again to be the most similar. Although only the pbe functional fails in describing the same order of states as ADC(2.5) and EOM-CCSD, the gap between the $n\pi\sigma \rightarrow 3s$ and $n\pi\sigma \rightarrow \pi^*$ transitions with 0.2 eV and 0.14 eV for b3lyp and pbe0 is quite low. Cam-b3lyp predicts an energy gap of 0.42 eV, closer to the energy gap predicted by ADC(2.5) and EOM-CCSD—therefore, this functional was chosen to simulate the absorption spectrum of the first band, incorporating the first three states.

Our calculations agree well with those of Schalk *et al.*,³ though their predicted vertical excitation energies are, in general, about 0.2–0.4 eV lower.

V. DISCUSSION

A. 23DHF

1. The $\pi\pi^*$ -transition around 6 eV

The first band from 5.2 eV to 6.5 eV is very broad, spanning 1.2 eV. The broadness of this band indicates a valence state. Comparing this with the vertical excitations displayed in [Table I](#), this band likely corresponds to the $\pi \rightarrow \pi^*$ transition and the lower-lying Rydberg states, likely intensely vibronically coupled (see green lines in [Fig. 3](#)). The simulation of the absorption spectrum from a nuclear ensemble using cam-b3lyp/aug-cc-pVDZ from 500 initial geometries, incorporating the first 6 states, is shown in red. This simulation reproduces well the overall shape of the first absorption band, confirming that this band results from a superposition of the $\pi \rightarrow 3p_y$ and $\pi \rightarrow \pi^*$ transitions, which are likely coupled.

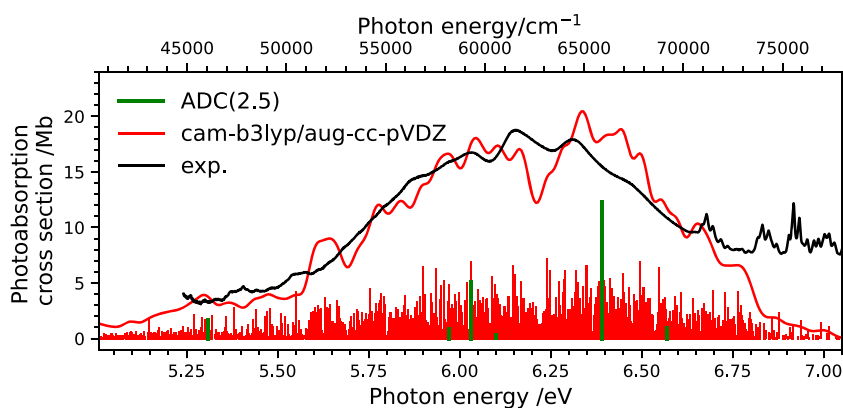


FIG. 3. Experimental absorption spectrum of 23DHF (black) and simulation of the absorption spectrum with cam-b3lyp/aug-cc-pVDZ. The individual transitions of this simulation, binned into 3000 bins, are displayed in red. The positions and assignments of vertical excitation energies at the ADC(2.5)/aug-cc-pVDZ level (C_1 geometry) are plotted as green lines, scaled by their relative oscillator strengths.

2. Rydberg states above 6.50 eV

The transition energy of an unperturbed Rydberg state can be calculated via

$$E_{\delta} = IE - \frac{R}{(n - \delta)^2}, \quad (1)$$

where IE is the ionization energy (8.38 eV for 23DHF³²), R is the Rydberg constant for C_4H_6O (13.605 586 4 eV), n is the principal quantum number, and δ is the quantum defect associated with a particular Rydberg series. For ns , np , nd , and nf series, δ typically has values in the ranges of (0.8–1.0), (0.4–0.7), (–0.2 to 0.2), and (–0.2 to 0.2), respectively.^{1,39} Using the Rydberg formula, we assign the peaks between 6.6 eV and 7.2 eV to $n = 3$ Rydberg series with quantum defects ranging from 0.18 to –0.2 eV, identifying them as either d- or f-Rydberg states (see Fig. 4). This coincides well with the vertical excitation energies estimated with various methods in Table I. The band between 7.15 eV and 7.35 eV probably corresponds to the $n = 4$ p-Rydberg series, and the peaks at higher energy to $n \geq 4$ s-, p-, d-, and f-Rydberg transitions.

The vibrational envelope of these Rydberg states differs both for states with the same quantum defect as well as for states with the same principal quantum number. This is apparently surprising, since the atomic-like picture of a Rydberg electron suggests that it is essentially unperturbed by the ionic core and therefore unaffected by the vibrational excitation of the ionic core, which drives the vibrational progression. The atomic-like picture is strictly valid when both the principal quantum number (say, $n > 3$) and the angular momentum (small quantum defect) are large.

Let us see which vibrational progressions are likely at play here. As stated earlier, the neutral ground state displays a double-well structure along the ring-puckering coordinate, with two C_1 -minima separated by a low C_s -structure barrier. For the cation,

the situation is likely similar. In fact, the cam-b3lyp/aug-cc-pVTZ optimized ground state structure of the 23DHF cation still is C_1 -symmetric (C_s -symmetric structure has one imaginary frequency), but the out-of-plane dihedral angle CH–O–CH₂–CH₂ is reduced from 21° for the neutral to 0.3° for the cation (see Fig. 1 of the supplementary material). Other bond lengths and angles remain unchanged, showing that the largest geometry change is the ring-puckering motion leading to planarity, corresponding to ν_{27} . The vibrational structure on top of each peak with $n = 3$ is therefore assigned to a ring puckering motion progression ν_{27} (see Table 6 of the supplementary material), agreeing with the measured spacing of 140 cm^{-1} – 110 cm^{-1} .

Since $n = 3$ Rydberg electrons in polyatomic molecules cannot be considered as strictly atomic-like and free of perturbations by the ionic core, the vibrational envelope is expected to differ for Rydberg states of different angular momenta (quantum defect). Rydberg states with $n > 3$ are more atomic-like, but their fine structure (levels of different angular momenta) is more compact, leading to overlapping bands and obscuring of the vibrational envelope.

It should be noted that the difference between the cation and neutral geometry also means a weak Franck–Condon-overlap, explaining the low absorption cross section of these Rydberg series. Absorption by CO impurities is also observed at 8.02 eV, 8.20 eV, and 8.40 eV (attributed in gray in Fig. 4). The carbon monoxide molecule is formed upon photolysis of 23DHF and remains long enough in the interaction region to absorb a second photon. The sharp peaks visible in Fig. 1 (top) above the ionization potential of 23DHF correspond to the strong $X \rightarrow A$ transitions of CO.^{40,41} From the absorption spectrum, the relative CO column density has been estimated to be less than 0.5% for both the 23DHF and 25DHF samples, well below our estimated precision. No further correction has been applied to the determined cross section.

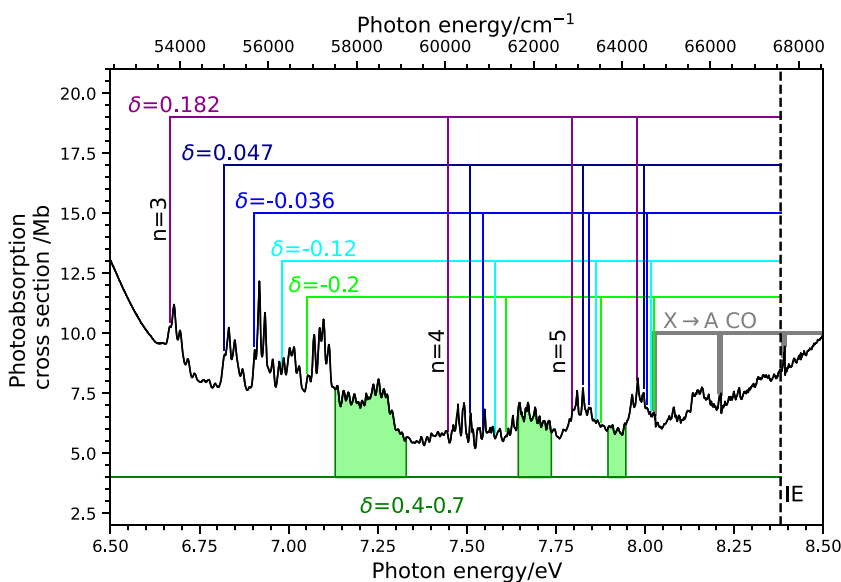


FIG. 4. Experimental absorption spectra of 23DHF from 6.5 eV to 8.5 eV with assignments of Rydberg states. The vertical dashed line corresponds to the ionization energy (IE) of 23DHF.³² Assignments of transitions into the d/f-Rydberg manifolds are displayed above the absorption spectrum, whereas transitions into the p-Rydberg manifold are assigned below the experimental absorption spectrum as green areas. Assignments in gray correspond to absorption of the impurity CO.

B. 25DHF

With four bands, the spectroscopy of 25DHF is significantly more difficult to disentangle than that of 23DHF. A guideline is provided by the present calculations, showing that the geometry of this molecule remains essentially unchanged upon removal of an electron (see Fig. 2 of the [supplementary material](#)). Hence, transitions from the ground state to atomic-like Rydberg series are expected to form narrow and intense bands. In contrast, the equilibrium geometries of the ground and valence excited states likely differ markedly and broad bands are expected for the corresponding transitions.

1. Band 1

The first absorption band of 25DHF (black line in Fig. 5), spanning from 5.50 eV to 6.75 eV, consists of a broad band with a clear vibrational progression visible on the lower-energy side. The broadness of this feature indicates a valence transition and corresponds likely to the vibronically coupled $n\pi\sigma \rightarrow \pi^*$ and $n\pi\sigma \rightarrow 3s$ -transitions and possibly 3p transitions. We simulated the spectrum from 500 individual geometries with cam-b3lyp/aug-cc-pVDZ including the first 3 states (red in Fig. 5, shifted by 0.26 eV). The shape of the simulated spectrum is in excellent agreement with the experimental spectrum and even reproduces the two peaks at 6.23 eV and 6.41 eV. Vibrational progressions cannot be predicted by nuclear ensemble methods,⁴² and any peak agreement here is only coincidental.

The vibrational progression has a spacing of 330 cm^{-1} . This spacing does not correspond to any frequency of 25DHF (see Table 7 of the [supplementary material](#)). The closest frequency would be an A_2 ring torsion at 394 cm^{-1} . Such a transition is, however, symmetry forbidden. Three different assignment possibilities are considered here: (a) Through vibronic coupling, A_2 -modes become accessible and the observed vibrational progression corresponds to the ν_{14} , the A_2 -symmetric ring torsion. (b) The progression could be a difference band. A candidate is the difference band of two B_2 vibrations, ν_{25} (CH_2 rock at 1011.2 cm^{-1}) and ν_{26} ($\gamma\text{CC-H}$ wag at 661.2 cm^{-1}), resulting in a symmetry of this difference band of A_1 . This difference frequency is therefore symmetry-allowed. However, such combination bands are usually associated with stronger individual mode progressions (of both ν_{25} and ν_{26}), making this

hypothesis unlikely. (c) The third possibility is that this is not a single vibrational progression, but the superposition of two progressions, as indicated in Fig. 5, with a spacing of 663 cm^{-1} and 658 cm^{-1} , respectively. This spacing aligns well with ν_{26} ($\gamma\text{CC-H}$ wag of B_2 -symmetry at 661.2 cm^{-1}), and the difference between those two vibrational progressions could correspond to one quantum of ν_{14} (A_2 ring torsion at 394 cm^{-1}). The product of the A_2 and B_2 irreducible representations is B_1 and is therefore symmetry-allowed. Unfortunately, since the absorption spectrum could not be recorded below 5.56 eV, the origin of the vibrational progression cannot be determined.

2. Band 2

Band 2 spans around 0.6 eV, and starts with one intense, sharp peak at 6.79 eV, followed by several structured peaks (see Fig. 6). The sharpness of this peak indicates that this is likely a transition with Rydberg character. However, as this peak is still broad compared with the Rydberg series observed in 23DHF, this is not an atomic-like Rydberg transition, but the electron remains perturbed by the core. We shall refer to such a state as having Rydberg character. According to our calculations, both the neutral and the cation are C_{2v} -symmetric and hardly differ in their geometry (see Fig. 2 of the [supplementary material](#))—in agreement with the He(I) photoelectron spectrum, which displays a sharp and narrow peak at the ionization potential.^{43,44} Therefore, for atomic-like Rydberg states, only three peaks corresponding to the origin bands of the three bright electronic states in this energy range ($n\pi\sigma \rightarrow p_x$, $n\pi\sigma \rightarrow 3p_z$, and $n\pi\sigma \rightarrow 3d_{xz}$) are expected. Instead, the spectrum is structured and fits surprisingly well with vibrational excitation of three Rydberg states (see Fig. 6). Even though the geometry of the Rydberg state should be similar to the neutral/cationic C_{2v} -structure, if these Rydberg states relax ultrafast to lower-lying electronic states, this not only would broaden these bands but could also lead to more structures.⁴⁵ In the following, we tentatively assign the observed bands using the measured vibrations of the neutral ground state. A more complete assignment would require, e.g., simulating the VUV spectrum using a model Hamiltonian,⁴⁵ which is beyond the scope of this paper.

Both ADC(2) and EOM-CCSD calculations predict that the next two higher-lying symmetry-allowed $n\pi\sigma \rightarrow p_x$ and $n\pi\sigma$

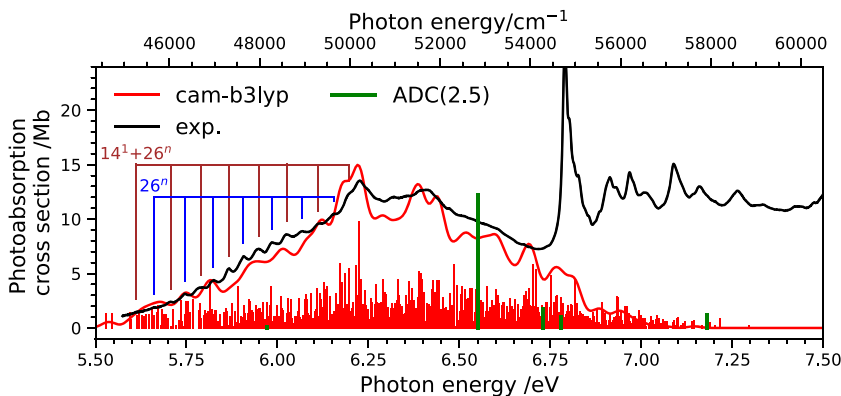


FIG. 5. Experimental absorption spectrum of 25DHF (black) and simulation of the absorption spectrum with cam-b3lyp/aug-cc-pVDZ (red), shifted by 0.26 eV. The individual transitions of the simulation binned into 3000 bins are displayed in red. The positions and assignments of vertical excitation energies at the ADC(2.5)/aug-cc-pVDZ level are plotted as green lines, scaled by their relative oscillator strengths.

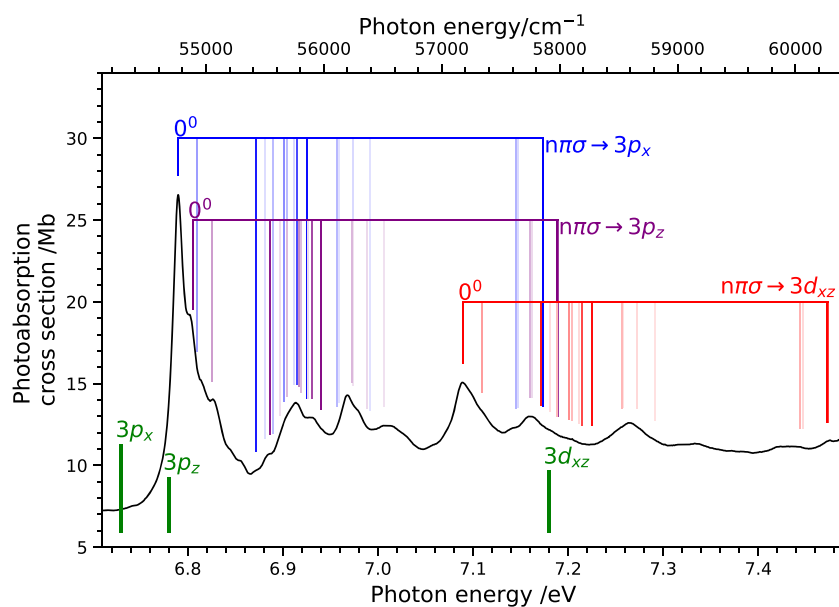


FIG. 6. Experimental absorption spectrum of 25DHF (black) from 6.7 eV to 7.7 eV. The vibrational progressions of the $n\pi\sigma \rightarrow 3p_x$, $n\pi\sigma \rightarrow 3p_z$, and $n\pi\sigma \rightarrow 3d_{xz}$ are based on the frequencies reported by Klots and Collier,³⁵ where only frequencies with a relative intensity of >0.07 have been considered. The transparency of each line represents the relative intensity, with the most intense lines being the least transparent. The positions and assignments of vertical excitation energies at the ADC(2.5)/aug-cc-pVDZ level are plotted as green lines, scaled by their relative oscillator strengths.

$\rightarrow 3p_z$ transitions are apart by only 0.05 eV and 0.1 eV, respectively. Attributing the peak at 6.79 eV to the $n\pi\sigma \rightarrow 3p_x$ transition (which has more oscillator strength), the difference to the peak/shoulder at 6.80 eV is too small to correspond to a vibrational excitation (122 cm^{-1} , lowest ring-puckering transition ν_{27} at 163 cm^{-1} ; see Table 7 of the [supplementary material](#)). We therefore attribute this peak to the $n\pi\sigma \rightarrow 3p_z$ transition. The following peaks up to 7.05 eV then correspond to vibrational excitation in the $n\pi\sigma \rightarrow 3p_x$ and $n\pi\sigma \rightarrow 3p_z$ -states. To guide the eye as to the assignments of the other broad peaks to vibrational transitions, the comb lines in Fig. 6 show the attribution of the 0^0 -transition superimposed with the frequencies reported by Klots *et al.*,³⁵ where the transparency reflects the relative transition strength of these frequencies. The peak at 7.08 eV corresponds to the next symmetry-allowed $n\pi\sigma \rightarrow 3d_{xz}$ transition. ADC(2.5) and EOM-CCSD predict this transition to be 0.1 eV and 0.28 eV

higher, which is still within the uncertainties of ADC(2.5)²⁴ and EOM-CCSD.⁸

3. Band 3

Band 3 is again broad, spanning from 7.4 eV to 8.0 eV, showing three main broad peaks at 7.55 eV, 7.69 eV, and 7.86 eV (see Fig. 7). The broadness indicates that this is the second transition of valence character, and we therefore assign it to the $n\pi \rightarrow \pi^*$ -transition. The predicted position of this transition by ADC(2.5) and EOM-CCSD is about 0.4 eV higher, indicating that this transition is likely intensely coupled to the lower $n\pi\sigma \rightarrow 3d_{xy}$ and $n\pi\sigma \rightarrow 3d_z^2$ transitions, which would be responsible for the three main broad features. Part of the vibrational progression around 8.0 eV and 8.2 eV corresponds to the X \rightarrow A transition of CO, an impurity produced upon VUV photolysis of 25DHF.

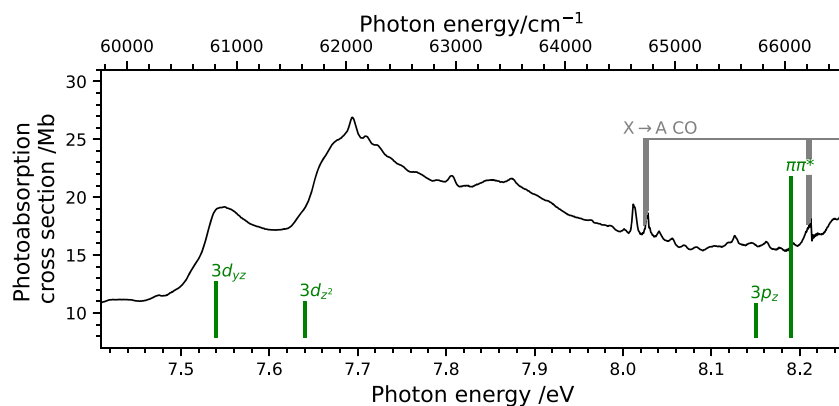


FIG. 7. Experimental absorption spectrum of 25DHF (black) from 7.4 eV to 8.25 eV. Sharp peaks between 8.0 eV and 8.1 eV are assigned to the $X^1\Sigma^+ \rightarrow A^1\Pi$ transition of the impurity CO.⁴⁰ The positions and assignments of vertical excitation energies at the ADC(2.5)/aug-cc-pVDZ level are plotted as green lines, scaled by their relative oscillator strengths.

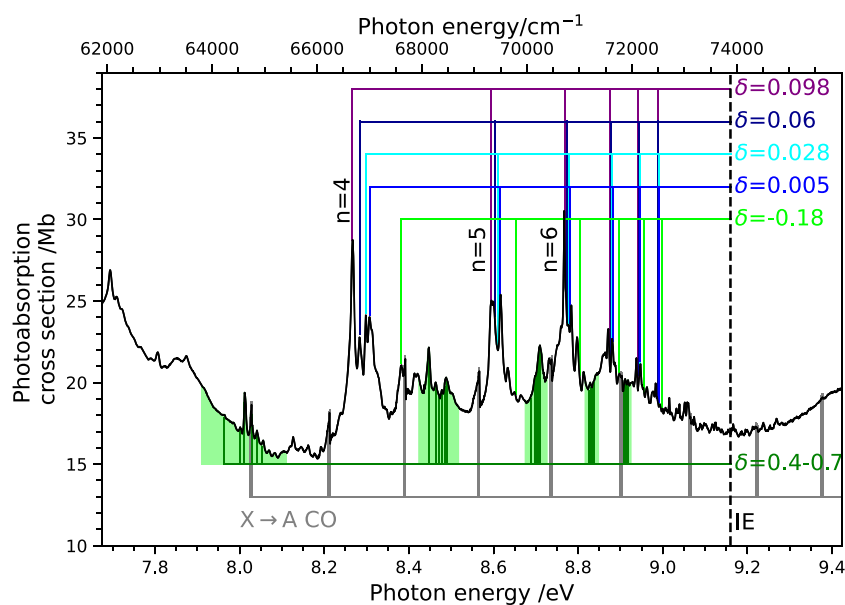


FIG. 8. Experimental absorption spectra of 25DHF from 7.6 eV to 9.4 eV with assignments of Rydberg states. The vertical dashed line corresponds to the ionization energy (IE) of 25DHF.³² Assignments of transitions into the d/f-Rydberg manifolds are displayed above the absorption spectrum, whereas transitions into the p-Rydberg manifold are assigned below the experimental absorption spectrum. Assignments in gray correspond to absorption of the photoproduct impurity CO.

4. Band 4

Above 8.2 eV and up to the ionization energy (IE), the absorption spectrum consists of several sharp peaks, grouped into clusters (see Fig. 8). These correspond to Rydberg series. As the geometry remains unchanged upon removal of an electron (see Fig. 2 of the [supplementary material](#)), vibrationally excited Rydberg states are not expected.

Using Eq. (1) with the ionization energy of 25DHF (IE = 9.16 eV³²) and starting from $n = 4$, five Rydberg series with δ ranging between -0.18 and 0.098 can be identified. These values are typical for d- and f-Rydberg states. From symmetry arguments, $d_{x^2-y^2}$ and d_{xy} are forbidden; therefore, these five Rydberg series consist of both d- and f-Rydberg series. Concerning p-Rydberg series, the p_y transition is symmetry forbidden, and we would therefore expect two p-Rydberg series with a δ between 0.4 and 0.7 (see the green shaded area in Fig. 8). Several Rydberg-series can be anticipated (see the [supplementary material](#) for the quantum defects associated with each peak). The vibrational progression starting around 8 eV has a spacing of around 111 cm^{-1} , which could correspond to the ring-pucker vibration ν_{27} . Peaks assigned in gray correspond to the $X \rightarrow A$ transition of CO, an impurity produced upon photolysis of 25DHF. The low-intensity peaks slightly above the ionization energy correspond to autoionizing Rydberg states converging toward excited states of the cation.

VI. SUMMARY

The first absorption bands of 23DHF and 25DHF are quite similar and correspond in both cases to a broad valence transition from 5.5 eV to 6.7 eV, attributed to the excitation of an electron from the HOMO to an unoccupied orbital with π^* character, coupled to the lower-lying Rydberg states. Due to the different symmetry of 23DHF (C_1) and 25DHF (C_{2v}), the next bands differ vastly

from each other: in 23DHF, we observe only Rydberg transitions with a ring-puckering vibrational progression converging to the ionization energy. In neutral 23DHF, one of the CH_2 -groups is distorted out of plane, whereas the 23DHF cation is nearly planar. As the geometry of Rydberg states is cation-like, this difference in geometry leads to a poor Franck-Condon overlap, explaining the low absorption cross sections of the Rydberg transitions between 6.8 eV and 8.4 eV. The quantum defects of these Rydberg transitions range from 0.182 to -0.2 and are attributed to d- and f-Rydberg series.

The geometry of 25DHF, on the other hand, remains unchanged upon ionization, and the peaks attributed to $n\pi\sigma \rightarrow 3p_x$, $n\pi\sigma \rightarrow 3p_z$, and $n\pi\sigma \rightarrow 3d_{xz}$ transitions with vibrational excitation following the first valence transition have a high absorption cross section. These peaks are sharp compared to the first valence transition, but broad compared to the higher-energetic Rydberg series converging to the ionization energy, showing that these Rydberg states are still perturbed by the ionic core or by a valence state. Moreover, in 25-DHF, both the HOMO and HOMO-1 have π -character, and a second valence transition into a π^* -orbital from 7.4 eV to 8.2 eV is observed. Starting from 8.2 eV and converging to the ionization energy, just as in 23DHF, several Rydberg transitions with quantum defects ranging from 0.098 to -0.18 are assigned to d- and f-Rydberg series.

The VUV absorption spectra of both isomeric molecules are contaminated with the $X \rightarrow A$ signature of carbon mono-oxide (CO), produced upon VUV photolysis and remaining long enough in the interaction region to absorb another VUV photon.

The here presented theoretical treatment allows us to unravel the essential spectroscopic features of 23 and 25DHF. Nevertheless, our results reveal a complex situation where both valence and Rydberg characters are mixed and likely strongly vibronically coupled, similar to furan.⁴⁶⁻⁴⁸ We hope that this observation will stimulate future theoretical research that addresses this question specifically.

SUPPLEMENTARY MATERIAL

See the [supplementary material](#) for the optimized ground state structures, frequencies, further calculations of vertical excitations and peak positions, and assignments.

ACKNOWLEDGMENTS

The authors are grateful to the technical staff of the SOLEIL Synchrotron Radiation Facility for smoothly running the facility under Project No. 20190076. The authors also thank D. Guay and D. Moffat for their relentless effort to ship the samples from Canada to France. A.R. thanks the Alexander von Humboldt Foundation and the Joint Centre for Extreme Photonic for financial support.

DATA AVAILABILITY

The data that support the findings of this study are available from the corresponding author upon reasonable request. The essential spectral information provided by the present work is available on the MPI/Mainz Spectral Data bank.⁴⁹

REFERENCES

- D. M. P. Holland, E. A. Seddon, A. B. Trofimov, E. V. Gromov, M. Wormit, A. Dreuw, T. Korona, N. De Oliveira, L. E. Archer, and D. Joyeux, "A study of the excited electronic states of normal and fully deuterated furan by photoabsorption spectroscopy and high-level *ab initio* calculations," *J. Mol. Spectrosc.* **315**, 184–195 (2015).
- A. Giuliani, P. Limão-Vieira, D. Duflot, A. R. Milosavljevic, B. P. Marinkovic, S. V. Hoffmann, N. Mason, J. Delwiche, and M.-J. Hubin-Franskin, "Electronic states of neutral and ionized tetrahydrofuran studied by VUV spectroscopy and *ab initio* calculations," *Eur. Phys. J. D* **51**, 97–108 (2009).
- O. Schalk, T. Geng, T. Hansson, and R. D. Thomas, "The ring-opening channel and the influence of Rydberg states on the excited state dynamics of furan and its derivatives," *J. Chem. Phys.* **149**, 084303 (2018).
- N. De Oliveira, M. Roudjane, D. Joyeux, D. Phalippou, J.-C. Rodier, and L. Nahon, "High-resolution broad-bandwidth Fourier-transform absorption spectroscopy in the VUV range down to 40 nm," *Nat. Photonics* **5**, 149–153 (2011).
- L. Nahon, N. d. Oliveira, G. A. Garcia, J.-F. Gil, D. Joyeux, B. Lagarde, and F. Polack, "DESIRS: A state-of-the-art VUV beamline featuring high resolution and variable polarization for spectroscopy and dichroism at SOLEIL," *J. Phys.: Conf. Ser.* **425**, 122004 (2013).
- N. De Oliveira, D. Joyeux, M. Roudjane, J.-F. Gil, B. Pilette, L. Archer, K. Ito, and L. Nahon, "The high-resolution absorption spectroscopy branch on the VUV beamline DESIRS at SOLEIL," *J. Synchrotron Radiat.* **23**, 887–900 (2016).
- N. De Oliveira, D. Joyeux, D. Phalippou, J. C. Rodier, F. Polack, M. Vervloet, and L. Nahon, "A Fourier transform spectrometer without a beam splitter for the vacuum ultraviolet range: From the optical design to the first UV spectrum," *Rev. Sci. Instrum.* **80**, 043101 (2009).
- Y. Shao, Z. Gan, E. Epifanovsky, A. T. B. Gilbert, M. Wormit, J. Kussmann, A. W. Lange, A. Behn, J. Deng, X. Feng, D. Ghosh, M. Goldey, P. R. Horn, L. D. Jacobson, I. Kaliman, R. Z. Khaliullin, T. Kus, A. Landau, J. Liu, E. I. Proynov, Y. M. Rhee, R. M. Richard, M. A. Rohrdanz, R. P. Steele, E. J. Sundstrom, H. L. Woodcock, P. M. Zimmerman, D. Zuev, B. Albrecht, E. Alguire, B. Austin, G. J. O. Beran, Y. A. Bernard, E. Berquist, K. Brandhorst, K. B. Bravaya, S. T. Brown, D. Casanova, C.-M. Chang, Y. Chen, S. H. Chien, K. D. Closser, D. L. Crittenden, M. Diedenhofen, R. A. DiStasio, H. Do, A. D. Dutoi, R. G. Edgar, S. Fatehi, L. Fusti-Molnar, A. Ghysels, A. Golubeva-Zadorozhnaya, J. Gomes, M. W. D. Hanson-Heine, P. H. P. Harbach, A. W. Hauser, E. G. Hohenstein, Z. C. Holden, T.-C. Jagau, H. Ji, B. Kaduk, K. Khistyayev, J. Kim, J. Kim, R. A. King, P. Klunzinger, D. Kosenkov, T. Kowalczyk, C. M. Krauter, K. U. Lao, A. D. Laurent, K. V. Lawler, S. V. Levchenko, C. Y. Lin, F. Liu, E. Livshits, R. C. Lochan, A. Luenser,
- P. Manohar, S. F. Manzer, S.-P. Mao, N. Mardirossian, A. V. Marenich, S. A. Maurer, N. J. Mayhall, E. Neuscamman, C. M. Oana, R. Olivares-Amaya, D. P. O'Neill, J. A. Parkhill, T. M. Perrine, R. Peverati, A. Prociuk, D. R. Rehn, E. Rosta, N. J. Russ, S. M. Sharada, S. Sharma, D. W. Small, A. Sodt, T. Stein, D. Stück, Y.-C. Su, A. J. W. Thom, T. Tsuchimochi, V. Vanovschi, L. Vogt, O. Vydrov, T. Wang, M. A. Watson, J. Wenzel, A. White, C. F. Williams, J. Yang, S. Yeganeh, S. R. Yost, Z.-Q. You, I. Y. Zhang, X. Zhang, Y. Zhao, B. R. Brooks, G. K. L. Chan, D. M. Chipman, C. J. Cramer, W. A. Goddard, M. S. Gordon, W. J. Hehre, A. Klamt, H. F. Schaefer, M. W. Schmidt, C. D. Sherrill, D. G. Truhlar, A. Warshel, X. Xu, A. Aspuru-Guzik, R. Baer, A. T. Bell, N. A. Besley, J.-D. Chai, A. Dreuw, B. D. Dunietz, T. R. Furlani, S. R. Gwaltney, C.-P. Hsu, Y. Jung, J. Kong, D. S. Lambrecht, W. Liang, C. Ochsenfeld, V. A. Rassolov, L. V. Slipchenko, J. E. Subotnik, T. Van Voorhis, J. M. Herbert, A. I. Krylov, P. M. W. Gill, and M. Head-Gordon, "Advances in molecular quantum chemistry contained in the Q-Chem 4 program package," *Mol. Phys.* **113**, 184–215 (2015).
- R. G. Parr and W. Yang, *Density-Functional Theory of Atoms and Molecules* (Oxford University Press, New York, 1989).
- P. J. Stephens, F. J. Devlin, C. F. Chabalowski, and M. J. Frisch, "*Ab initio* calculation of vibrational absorption and circular dichroism spectra using density functional force fields," *J. Phys. Chem.* **98**, 11623–11627 (1994).
- K. Kaufmann, W. Baumeister, and M. Jungen, "Universal Gaussian basis sets for an optimum representation of Rydberg and continuum wavefunctions," *J. Phys. B: At., Mol. Opt. Phys.* **22**, 2223–2240 (1989).
- A. Dreuw and M. Head-Gordon, "Single-reference *ab initio* methods for the calculation of excited states of large molecules," *Chem. Rev.* **105**, 4009–4037 (2005).
- T. Yanai, D. P. Tew, and N. C. Handy, "A new hybrid exchange-correlation functional using the Coulomb-attenuating method (CAM-B3LYP)," *Chem. Phys. Lett.* **393**, 51–57 (2004).
- J. P. Perdew, K. Burke, and M. Ernzerhof, "Generalized gradient approximation made simple," *Phys. Rev. Lett.* **77**, 3865–3868 (1996).
- C. Adamo and V. Barone, "Toward reliable density functional methods without adjustable parameters: The PBE0 model," *J. Chem. Phys.* **110**, 6158–6170 (1999).
- A. B. Trofimov, G. Stelter, and J. Schirmer, "A consistent third-order propagator method for electronic excitation," *J. Chem. Phys.* **111**, 9982–9999 (1999).
- P. H. P. Harbach, M. Wormit, and A. Dreuw, "The third-order algebraic diagrammatic construction method (ADC(3)) for the polarization propagator for closed-shell molecules: Efficient implementation and benchmarking," *J. Chem. Phys.* **141**, 064113 (2014).
- M. Wormit, D. R. Rehn, P. H. P. Harbach, J. Wenzel, C. M. Krauter, E. Epifanovsky, and A. Dreuw, "Investigating excited electronic states using the algebraic diagrammatic construction (ADC) approach of the polarisation propagator," *Mol. Phys.* **112**, 774–784 (2014).
- A. B. Trofimov and J. Schirmer, "An efficient polarization propagator approach to valence electron excitation spectra," *J. Phys. B: At., Mol. Opt. Phys.* **28**, 2299–2324 (1995).
- A. B. Trofimov, G. Stelter, and J. Schirmer, "Electron excitation energies using a consistent third-order propagator approach: Comparison with full configuration interaction and coupled cluster results," *J. Chem. Phys.* **117**, 6402–6410 (2002).
- J. Schirmer, "Beyond the random-phase approximation: A new approximation scheme for the polarization propagator," *Phys. Rev. A* **26**, 2395–2416 (1982).
- H. Sekino and R. J. Bartlett, "A linear response, coupled-cluster theory for excitation energy," *Int. J. Quantum Chem.* **26**, 255–265 (1984).
- D. E. Woon and T. H. Dunning, "Gaussian basis sets for use in correlated molecular calculations. V. Core-valence basis sets for boron through neon," *J. Chem. Phys.* **103**, 4572–4585 (1995).
- P.-F. Loos and D. Jacquemin, "Is ADC(3) as accurate as CC3 for valence and Rydberg transition energies?," *J. Phys. Chem. Lett.* **11**, 974–980 (2019); .
- R. L. Martin, "Natural transition orbitals," *J. Chem. Phys.* **118**, 4775–4777 (2003).
- G. Gate, R. Szabla, M. R. Haggmark, J. Šponer, A. L. Sobolewski, and M. S. de Vries, "Photodynamics of alternative DNA base isoguanine," *Phys. Chem. Chem. Phys.* **21**, 13474 (2019).
- S. Farahani, B. N. Frandsen, H. G. Kjaergaard, and J. R. Lane, "Simulated electronic absorption spectra of sulfur-containing molecules present in Earth's

- atmosphere," *J. Phys. Chem. A* **123**, 6605–6617 (2019), part of virtual special issue "Leo Radom Festschrift".
- ²⁸S.-a. Hua, M. Cattaneo, M. Oelschlegel, M. Heindl, L. Schmid, S. Dechert, O. S. Wenger, I. Siewert, L. González, and F. Meyer, "Electrochemical and photophysical properties of ruthenium(II) complexes equipped with sulfurated bipyridine ligands," *Inorg. Chem.* **59**, 4972–4984 (2020).
- ²⁹R. Sarkar, M.-c. Heitz, G. Royal, and M. Boggio-Pasqua, "Electronic excited states and UV-VIS absorption spectra of the dihydropyrene/cyclophanediene photochromic couple: A theoretical investigation," *J. Phys. Chem. A* **124**, 1567–1579 (2020).
- ³⁰M. Barbatti, M. Ruckebauer, F. Plasser, J. Pittner, G. Granucci, M. Persico, and H. Lischka, "Newton-X: A surface-hopping program for nonadiabatic molecular dynamics," *Wiley Interdiscip. Rev.: Comput. Mol. Sci.* **4**, 26–33 (2014).
- ³¹M. Barbatti, G. Granucci, M. Ruckebauer, F. Plasser, R. Crespo-Otero, J. Pittner, M. Persico, and H. Lischka, "Newton-X: A package for Newtonian dynamics close to the crossing seam," Version 2, **2016**, www.newtonx.org.
- ³²B. Yang, J. Wang, T. A. Cool, N. Hansen, S. Skeen, and D. L. Osborn, "Absolute photoionization cross-sections of some combustion intermediates," *Int. J. Mass Spectrom.* **309**, 118–128 (2012).
- ³³W. H. Green, "Ring-puckering vibration of 2,3-dihydrofuran," *J. Chem. Phys.* **50**, 1619–1621 (1969).
- ³⁴D. Autrey and J. Laane, "Far-infrared spectra, *ab initio* calculations, and the ring-puckering potential energy function of 2,3-dihydrofuran," *J. Phys. Chem. A* **105**, 6894–6899 (2001).
- ³⁵T. D. Klots and W. B. Collier, "Vibrational assignment and analysis for 2,3-dihydrofuran and 2,5-dihydrofuran," *Spectrochim. Acta, Part A* **50**, 1725–1748 (1994).
- ³⁶J. c. López, G. Włodarczak, and J. Demaison, "The millimeter-wave spectrum of 2,3-dihydrofuran," *J. Mol. Spectrosc.* **180**, 337–344 (1996).
- ³⁷T. Ueda and T. Shimanouchi, "Ring-puckering motion of 2,5-dihydrofuran," *J. Chem. Phys.* **47**, 4042–4047 (1967).
- ³⁸T. Ueda and T. Shimanouchi, "Near-infrared band progressions of ring molecules and ring-puckering motion," *J. Chem. Phys.* **47**, 5018–5030 (1967).
- ³⁹T. Ridley, K. P. Lawley, and R. J. Donovan, "A study of the Rydberg states of furan (C₄H₄O) and deuterated furan (C₄D₄O) using mass-resolved (2+1) and (3+1) resonance enhanced multiphoton ionization," *Phys. Chem. Chem. Phys.* **6**, 5304–5312 (2004).
- ⁴⁰M. L. Niu, E. J. Salumbides, D. Zhao, N. De Oliveira, D. Joyeux, L. Nahon, R. W. Field, and W. Ubachs, "High resolution spectroscopy and perturbation analysis of the CO A¹Π-X¹Π⁺ (0,0) and (1,0) bands," *Mol. Phys.* **111**, 2163–2174 (2013).
- ⁴¹M. L. Niu, E. J. Salumbides, A. N. Heays, N. De Oliveira, R. W. Field, and W. Ubachs, "Spectroscopy and perturbation analysis of the CO A¹Π-X¹Σ⁺ (2,0), (3,0) and (4,0) bands," *Mol. Phys.* **114**, 627–636 (2016).
- ⁴²R. Crespo-Otero and M. Barbatti, "Spectrum simulation and decomposition with nuclear ensemble: Formal derivation and application to benzene, furan and 2-phenylfuran," *Theor. Chem. Acc.* **131**, 1237 (2012).
- ⁴³M. Bloch, E. Heilbronner, T. B. Jones, and J. L. Ripoll, "Photoelectron spectra of unsaturated oxides II: 2,5-dihydrofuran derivatives," *Heterocycles* **11**, 443–454 (1978).
- ⁴⁴E. Heilbronner, M. Bloch, T. B. Jones, and J. L. Ripoll, "Photoelectron spectra of unsaturated oxides II, 2,5-dihydrofuran derivatives," *Heterocycles* **11**, 443 (1978).
- ⁴⁵S. P. Neville, A. Stolow, and M. S. Schuurman, "Vacuum ultraviolet excited state dynamics of the smallest ring, cyclopropane. I. A reinterpretation of the electronic spectrum and the effect of intensity borrowing," *J. Chem. Phys.* **149**, 144310 (2018).
- ⁴⁶E. V. Gromov, A. B. Trofimov, N. M. Vitkovskaya, J. Schirmer, and H. Köppel, "Theoretical study of the low-lying excited singlet states of furan," *J. Chem. Phys.* **119**, 737–753 (2003).
- ⁴⁷E. V. Gromov, A. B. Trofimov, N. M. Vitkovskaya, H. Köppel, J. Schirmer, H.-D. Meyer, and L. S. Cederbaum, "Theoretical study of excitations in furan: Spectra and molecular dynamics," *J. Chem. Phys.* **121**, 4585–4598 (2004).
- ⁴⁸E. V. Gromov, C. Lévesque, F. Gatti, I. Burghardt, and H. Köppel, "Ab initio quantum dynamical study of photoinduced ring opening in furan," *J. Chem. Phys.* **135**, 164305 (2011).
- ⁴⁹H. Keller-Rudek, G. K. Moortgat, R. Sander, and R. Sörensen, "The MPI-Mainz UV/VIS spectral atlas of gaseous molecules of atmospheric interest," *Earth Syst. Sci. Data* **5**, 365–373 (2013).